Available online at www.sciencedirect.com
SCIENCE DIRECT®
Deep-Sea Research I 51 (2004) 1541–1561
DEEP-SEA RESEARCH PART I
www.elsevier.com/locate/dsr

Net and gross O_2 production in the southern ocean from measurements of biological O_2 saturation and its triple isotope composition

Melissa B. Hendricks*, Michael L. Bender, Bruce A. Barnett

Department of Geosciences, Princeton University, Princeton, NJ 08544-1003, USA

Received 28 May 2003; accepted 15 June 2004
Available online 25 August 2004

Abstract

Mixed layer seawater samples from the Southern Ocean were analyzed for the triple oxygen isotope composition ($\delta^{17}O$ and $\delta^{18}O$) of dissolved O_2 and the ratio of [O_2] to [Ar]. $\delta^{17}O$ and $\delta^{18}O$ together constrain the mass independent anomaly in O_2, and hence the fraction of photosynthetic O_2 in the dissolved O_2 pool. Assuming oxygen in the mixed layer is at steady state, we calculate ratios of the gross photosynthetic O_2 production rate to the O_2 air–sea gas exchange rate, and ratios of net to gross O_2 production rates. With estimates of the O_2 gas exchange rate from a wind speed parameterization, we determine absolute in situ rates of gross and net O_2 production. Based on the net/gross production ratios and $\delta^{18}O$ of dissolved O_2, we calculate a value for the ^{18}O fractionation factor associated with marine respiration in the Southern Ocean mixed layer of 0.978 (an isotope effect of 22‰). The study regions cover latitudes between ~45°S and the ice edge at: (1) 175°E in December 1999, (2) 145°E in December 2000, and (3) 145°E in January 2001. At both meridians, gross O_2 production decreases to the south. At 145°E, rates of net O_2 production follow the same pattern, while at 175°E these rates are consistently low at all latitudes. In December, gross and net O_2 production rates are both higher at 145°E than at 175°E. Gross O_2 production at 145°E was similar in December and January, but net O_2 production decreased by ~50%. Net/gross C production ratios, calculated by scaling O_2 production rates, are lower than estimates of the ^{15}N *f*-ratio, determined as the ratio of $^{15}NO_3^-$ uptake to $^{15}NO_3^- + {}^{15}NH_4^+$ uptake in ^{15}N incubations. They are also lower than *ef*-ratios predicted by the model of Laws et al. (Global Biogeochem. Cycles 14 (2000a) 1231) at the temperatures of the Southern Ocean. The differences in the measurements could be due to natural interannual and spatial variability or the differences in metabolic rates measured and modeled, and the fundamental assumptions required by each technique.

1. Introduction

Because of its size, nutrient burden, and close link to the deep ocean, the surface Southern Ocean

*Corresponding author. Tel.: +1-609-258-2756; fax: +1-609-258-0796.
E-mail address: mhendric@princeton.edu (M.B. Hendricks).

0967-0637/$ - see front matter © 2004 Elsevier Ltd. All rights reserved.
doi:10.1016/j.dsr.2004.06.006

has the potential to exert a major influence on the global carbon cycle. Its role in this regard depends on gross production in the region and the fraction of fixed carbon that is exported to the deep ocean. Satellite images and fluorescence studies show many regions of the Southern Ocean are high in chlorophyll-*a*, one indication of high rates of C production (Moore and Abbott, 2000; Froneman et al., 2001; Arrigo et al., 1998). The other term affecting export, net/gross production, is more uncertain: recent studies (e.g. Laws et al., 2000a; Mengesha et al., 1998; Sambrotto and Mace, 2000) suggest a wide range of values. More work is needed to characterize these ratios and carbon fluxes and to understand their variability.

In this study, mixed layer water samples were collected on three crossings of the Southern Ocean during December 1999, December 2000, and January 2001. Samples were also collected on a cruise in the Eastern Bellingshausen Sea and the Drake Passage in March 2000. The purpose of this work is to determine rates of net O_2 production (N), gross O_2 production (G), and the ratios of net/gross O_2 production (N/G). For this purpose, we measure the biological O_2 saturation, which is O_2 saturation minus Ar saturation (Craig and Hayward, 1987; Emerson, 1987; Spitzer and Jenkins, 1989; Quay et al., 1993), and the triple oxygen isotope composition (^{16}O, ^{17}O, and ^{18}O) of dissolved O_2 (Luz and Barkan, 2000; Bender, 2000). We calculate absolute rates using gas exchange parameterizations based on wind speeds taken from reanalysis data (model results that are forced with local observations) of the National Center for Environmental Prediction (NCEP). Because this parameterization is not well characterized, rates of net and gross O_2 production are less accurately constrained than the N/G ratios, calculation of which does not require an estimate of the gas exchange coefficient. The N/G ratio is comparable to the *f*-ratio, defined by Eppley and Peterson (1979) as the ratio of new production to total primary production. We use the term "*f*-ratio" as a generic term to describe any measure of new, net, or export production divided by total or gross production. When comparing our results to results of other works, we apply precisely defined terms to each method.

2. Basis of method

The generalized equations used in this study are presented here, and a full derivation appears in the Appendix. We begin with a general equation to describe oxygen concentrations in the mixed layer and then move on to a discussion of the $\delta^{18}O$ system and, finally, the triple oxygen isotopes. When the mixed layer is at steady state, the O_2 concentration can be described by the following equation (Emerson, 1987):

$$h\frac{dC}{dt} = 0 = G - R + k(C_{sat} - C), \quad (1)$$

where h is the depth of the mixed layer in meters, C is the O_2 concentration (expressed here, for convenience, as mmol $O_2\,m^{-3}$), G is the gross rate of O_2 production by photosynthesis integrated over the depth of the mixed layer (mmol $O_2\,m^{-2}\,d^{-1}$), R is the rate of O_2 consumption by respiration also integrated over the depth of the mixed layer (mmol $O_2\,m^{-2}\,d^{-1}$), k is the gas exchange coefficient for O_2 ($m\,d^{-1}$) and C_{sat} is the saturation O_2 concentration (mmol $O_2\,m^{-3}$). The term $k(C_{sat}-C)$ is the net rate of gas exchange with the atmosphere.

Fig. 1a is a *generalized* vector diagram that shows how $\delta^{18}O$ of dissolved O_2 in the mixed layer ($\delta^{18}_{dis}O$) covaries with [O_2] for each process in Eq. (1). (We use the standard delta notation in units of per mil: $\delta^*O = (X^*/X^*_{std} - 1) \times 10^3$, where δ^*O is either $\delta^{17}O$ or $\delta^{18}O$ and X^* is the isotopic ratio ($^*O/^{16}O$) of the sample. X^*_{std} is the isotopic ratio of the standard, atmospheric O_2 in this study.) $\delta^{18}_{dis}O$ is generally close to 0 ($\equiv\delta^{18}O$ of atmospheric O_2). Marine photosynthesis produces O_2 that has the same isotopic composition as sea water (Guy et al., 1993), $\delta^{18}_wO = -22.96‰$. This is $\delta^{18}O$ of Standard Mean Ocean Water (SMOW) with atmospheric O_2 as the standard (Kroopnick and Craig, 1972). See the Appendix for details about this value. Thus, addition of photosynthetic O_2 causes an increase in [O_2] and a decrease in the $\delta^{18}O$. O_2 consumed during respiration has a lower $^{18}O/^{16}O$ ratio than the dissolved O_2. Respiration therefore results in an increase in $\delta^{18}_{dis}O$, while it lowers [O_2]. We take α^{18}_R, the ^{18}O fractionation factor for respiration, as 0.982 (Bender, 1990; Kiddon et al., 1993). The effect of gas exchange is

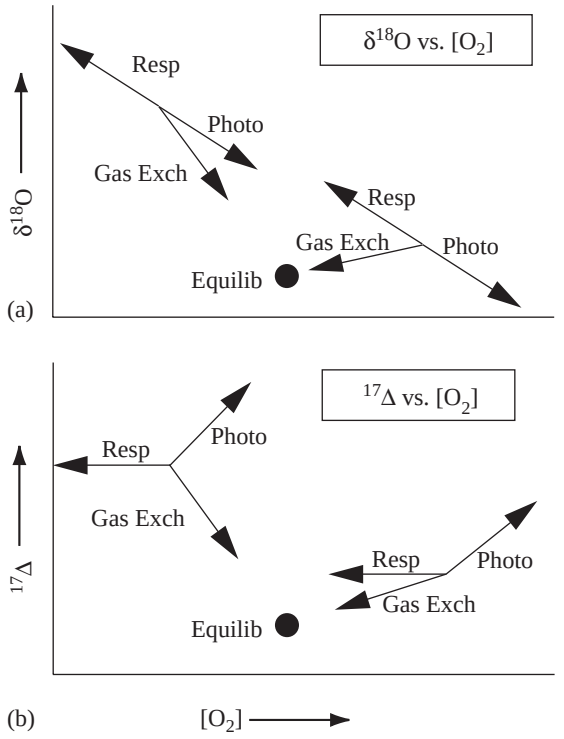

Fig. 1. General vector diagrams showing the effects of photosynthesis, respiration, and air–sea gas exchange on oxygen concentration and (a) $\delta^{18}O$ of dissolved O_2 (b) $^{17}\Delta$ of dissolved O_2. The circle marked "Equilib" represents isotopic and concentration equilibrium with the atmosphere.

always to push O_2 toward equilibrium with the atmosphere, in which $[O_2]$ equals the saturation concentration. Equilibrium $\delta^{18}O$ ($\delta^{18}_{sat}O$) lies between 0.7‰ and 0.85‰ at temperatures typical of the surface ocean (Benson and Krause, 1984; Kroopnick and Craig, 1972).

In the Appendix, we derive an equation, reproduced here, that relates $\delta^{18}_{dis}O$ to G/kC_{sat}, and C/C_{sat}. G/kC_{sat} equals the rate of gross O_2 production divided by the rate of O_2 invasion from the atmosphere. C/C_{sat} is the ratio of the concentration of dissolved O_2 to the saturation concentration of dissolved O_2. The derivation assumes steady state.

$$\delta^*_{dis}O/10^3 = \frac{(G/kC_{sat})(\delta^*_W O/10^3+1)+(\delta^*_{sat}O/10^3+1)}{(G/kC_{sat})+1-((G/kC_{sat})+1-(C/C_{sat}))(1-\alpha^*_R)}-1 \quad (2)$$

$\delta^{18}_{dis}O$ can also be written in terms of C/C_{sat} and N/G, the ratio of the rate of net O_2 production to the rate of gross O_2 production:

$$\delta^*_{dis}O/10^3 = \frac{(C/C_{sat}-1)(\delta^*_W O/10^3+1)+(N/G)(\delta^*_{sat}O/10^3+1)}{C/C_{sat}-1+N/G-(1-N/G)(C/C_{sat}-1)(1-\alpha^*_R)}-1. \quad (3)$$

These equations show that it is possible, in principle, to determine the G/kC_{sat} and N/G ratios from coupled measurements of $\delta^{18}_{dis}O$ and C/C_{sat}. Bender and Grande (1987) and Quay et al. (1993) both investigated this approach for measuring N/G. They showed that it works poorly because of uncertainties in α^{18}_R. N/G calculated using eq. (3) is highly sensitive to the exact value of α^{18}_R, especially when $\alpha^{18}_R \sim 1+\delta^{18}_W O/10^3$, as is the case for the oceanic mixed layer.

Now we move on to the triple oxygen isotope system, where the normal difference in $\delta^{17}O$ of any two compounds is nearly 0.5 times the difference in $\delta^{18}O$. With SMOW as a reference, all biologically produced O_2 has $\delta^{17}O \approx 0.5 \cdot \delta^{18}O$. Atmospheric O_2 is anomalous with respect to this trend: $\delta^{17}_{atm}O$ is less than $0.5 \cdot \delta^{18}_{atm}O$ by ~0.250‰. This anomaly is due to isotope exchange between O_2 and CO_2 in the stratosphere, which produces a change in $\delta^{17}O$ of O_2 that is larger than the change in $\delta^{18}O$ of O_2 (Thiemens et al., 1991, 1995; Yung et al., 1997; Luz et al., 1999; Lämmerzahl et al., 2002). Here we exploit this anomaly, following Luz and Barkan (2000), to investigate N/G ratios, as well as absolute values of these two rates.

The quantity $^{17}\Delta$, a measure of the mass-independent anomaly, is defined by Angert et al. (2003) as

$$^{17}\Delta/10^6 = \ln(X^{17}/X^{17}_{std}) - 0.516\ln(X^{18}/X^{18}_{std}), \quad (4)$$

which is equivalent to

$$^{17}\Delta/10^6 = \ln(\delta^{17}O/10^3+1) - 0.516\ln(\delta^{18}O/10^3+1). \quad (5)$$

Since $^{17}\Delta$ is always less than 0.250‰ in this paper, we use per meg notation (1000 per meg = 1‰).

When $\delta^{17}O$ and $\delta^{18}O$ are close to zero, as is true for our samples, $^{17}\Delta$ can be approximated as $\Delta^{17}O$:

$$^{17}\Delta/10^3 \approx \Delta^{17}O/10^3 = \delta^{17}O - 0.516 \cdot \delta^{18}O, \quad (6)$$

where 0.516 is the coefficient, or "slope", associated with ordinary dark respiration (cytochrome oxidase pathway: Angert et al., 2003), the dominant form of respiration. (See Angert et al. (2003), Miller (2002), and Young et al. (2002) for a full discussion of the difference between $^{17}\Delta$ and $\Delta^{17}O$.) The slope for respiration via the alternative pathway is 0.514 and for photorespiration is ~0.506 (Angert et al., 2003). For this data set, $^{17}\Delta$ is relatively insensitive to the exact value used for the slope because $\delta^{17}O$ and $\delta^{18}O$ values fall between 0 and 1‰.

Fig. 1b shows the general effect of each process on $^{17}\Delta$ of dissolved O_2 in the steady-state mixed layer ($^{17}\Delta_{dis}$). Marine photosynthesis adds O_2 with $^{17}\Delta_W = +249$ per meg, where atmospheric O_2 is the standard (Luz and Barkan, 2000). Therefore, photosynthesis causes $[O_2]$ and $^{17}\Delta_{dis}$ to rise. Respiration is mass dependent and the change in $\delta^{17}_{dis}O = 0.516$ times the change in $\delta^{18}_{dis}O$. Respiration forces $[O_2]$ to fall, but $^{17}\Delta_{dis}$ is unchanged (see Eq. (6)). Gas exchange again has the effect of forcing O_2 toward equilibrium with the atmosphere. The equilibrium $^{17}\Delta$ of dissolved O_2 ($^{17}\Delta_{sat}$) is +16 per meg (Luz and Barkan, 2000) and the equilibrium $[O_2]$ is, of course, the saturation concentration. Gas exchange may raise or lower $[O_2]$. It will always lower $^{17}\Delta_{dis}$ in waters to which photosynthetic O_2 has been added, and leave $^{17}\Delta_{dis}$ unchanged in waters that have no photosynthetic O_2.

When we assume the mixed layer is at a steady-state condition with respect to O_2, the general formula derived in the Appendix for $^{17}\Delta_{dis}$ is (Luz and Barkan, 2000)

$$^{17}\Delta_{dis} \approx \Delta^{17}O_{dis} = \frac{(G/kC_{sat})\Delta^{17}O_W + \Delta^{17}O_{sat}}{(G/kC_{sat}) + 1},$$

$$\frac{G}{kC_{sat}} = \frac{\Delta^{17}O_{sat} - \Delta^{17}O_{dis}}{\Delta^{17}O_{dis} - \Delta^{17}O_W}. \quad (7)$$

Eq. (7) shows that $^{17}\Delta_{dis}$ serves as a direct measure of the fraction of dissolved O_2 that came from photosynthetic production versus exchange with the atmosphere ($= G/kC_{sat}$). As an example, when the rates of gross O_2 production and O_2 invasion are equal ($G/kC_{sat} = 1$), $^{17}\Delta_{dis} \approx \Delta^{17}O_{dis} = 132.5$ per meg ($= (1 \cdot 249 + 16)/(1 + 1)$ per meg). Notice that, unlike $\delta^{18}_{dis}O$ in Eq. (2), $\Delta^{17}O_{dis}$ is independent of α_R and C/C_{sat}. $^{17}\Delta_{dis}$, the unapproximated term, is dependent on these properties, but the dependence is weak. For example, when $G/kC_{sat} = 0.3$ (a typical high-end value for these samples), $^{17}\Delta_{dis}$ varies by 3 per meg for a range in α^{18}_R from 0.975 to 0.985. $^{17}\Delta_{dis}$ varies by 2 per meg for a range in C/C_{sat} from 0.95 to 1.05. Even though the difference between $^{17}\Delta$ and $\Delta^{17}O$ is small for our data set, we use the unapproximated $^{17}\Delta$ and its formulae in the Appendix for all calculations.

From measurements of $^{17}\Delta_{dis}$ we determine the G/kC_{sat} ratio at each location and, then, a value for G, based on an estimate of kC_{sat}. C_{sat} is calculated from the temperature and salinity measured at the sample location and the O_2 solubility equation of Weiss (1970). k is determined at each sample location from an estimate of the average wind speed at 10 m and Wanninkhof's (1992) quadratic relationship between gas exchange rate and wind speed. Deriving an appropriate value of k is complicated by the fact that gas concentrations in the mixed layer depend on the recent history of wind speed rather than simply on the instantaneous wind speed at the time of sampling. The appropriate period over which to average the wind speed corresponds to the time required to cycle the entire mixed layer by gas exchange, which depends on the depth of the mixed layer as well as the gas exchange rate. From the work of Morrison et al. (2001), we estimate the depth of the mixed layer in our study region to be 40–60 m (however, variability is likely to be considerably greater than this range). The 10 m wind speeds from the NCEP reanalysis correspond to gas exchange coefficients ranging from 1.2 to 8.5 m d^{-1}, averaging ~5 m d^{-1} (NCEP reanalysis data provided by the NOAA-CIRES Climate Diagnostics Center, Boulder, CO, USA, from their Web site at www.cdc.noaa.gov/). Based on these considerations, we estimate that the mixed layer O_2 signal is integrated over ~10 days. We thus use the average wind speed at each location over the 10 days prior to the temporal midpoint of

each cruise. (Each transect was completed in fewer than 6 days.) We calculate the average gas exchange rate from this wind speed value. This average is then used to calculate net and gross production.

Like $\delta^{18}_{dis}O$, $^{17}\Delta_{dis}$ can be written in terms of N/G and C/C_{sat}.

$$^{17}\Delta_{dis} \approx \Delta^{17}O_{dis} = \frac{(C/C_{sat}-1)\Delta^{17}O_W + (N/G)\Delta^{17}O_{sat}}{(C/C_{sat})-1+(N/G)},$$

$$\frac{N}{G} \approx \left(\frac{C}{C_{sat}}-1\right)\frac{\Delta^{17}O_{dis}-\Delta^{17}O_W}{\Delta^{17}O_{sat}-\Delta^{17}O_{dis}}. \quad (8)$$

We determine N/G ratios from paired measurements of $^{17}\Delta_{dis}$ and C/C_{sat}. As discussed above, $\Delta^{17}O_{dis}$ is insensitive to the respiration fractionation factors and $^{17}\Delta_{dis}$, the unapproximated term, has a very small dependence on the respiratory fractionation factors. $^{17}\Delta_{dis}$ depends primarily on the coefficient of the last term in Eqs. (4) and (5), which is thought to be fairly constant for the various forms of respiration (Angert et al., 2003).

Absolute rates of net O_2 production are then calculated from the N/G ratios and the rates of gross O_2 production. This is mathematically equivalent to Eq. (1) rewritten as

$$N = kC_{sat}\left(\frac{C}{C_{sat}}-1\right). \quad (9)$$

The interpretation of $[O_2]$ is complicated by the fact that both warming (without a compensatory decrease in $[O_2]$) and bubble injection induce O_2 supersaturation (Craig and Hayward, 1987; Spitzer and Jenkins, 1989; Emerson, 1987; Quay et al., 1993). As well, atmospheric pressure variations cause gas solubilities to differ from those at one standard atmosphere pressure. Since the effects of air injection, temperature changes, and variations in atmospheric pressure on oxygen saturation anomalies are similar to the effects on argon saturation anomalies (Weiss, 1970; Craig and Hayward, 1987) and argon has no biological sources or sinks, measurements of argon saturation anomalies are used to remove physical contributions to the oxygen concentration. In this paper, we define the "biological oxygen saturation" as the O_2/Ar ratio divided by the O_2/Ar ratio at saturation, $([O_2]/[Ar])/([O_2]_{sat}/[Ar]_{sat})$. The denominator is simply a function of temperature and salinity. Biological oxygen saturation is used for C/C_{sat} in all equations. Then, the "biological oxygen supersaturation" is defined as O_2 supersaturation in excess of Ar supersaturation, which equals the biological oxygen saturation minus one. Here, we assume that [Ar] is at saturation. In fact, however, [Ar] is likely supersaturated by several percent in our samples, introducing a small, proportional error into the calculated values of net production and net/gross production.

3. General comparisons between $^{17}\Delta$ method and other measures of biological production

In order to compare our results with previous work, we need to convert rates of production determined by different approaches to a common currency. We choose to express rates as net C production and gross C production. The latter is defined as the production rate of organic C not subsequently lost to photorespiration. In the Southern Ocean, net C production has been estimated directly from the seasonal CO_2 drawdown during the US JGOFS Southern Ocean Study (Morrison et al., 2001). In other cases, net and gross C production are derived terms based on different, but related, rate measurements. At the outset, we are comparing rates determined with different methods that have large uncertainties, and that cannot be used to calculate carbon fluxes that are perfectly comparable.

We convert net O_2 production to net C production assuming a photosynthetic quotient of 1.4 (Laws, 1991). We convert $^{15}NO_3^-$ assimilation, measured by the particulate ^{15}N increase, to net C production assuming 30% of assimilated N is excreted as dissolved organic nitrogen (Bronk and Ward, 2000), and the Redfield C:N ratio of 6.6. Hence, net C production $= 6.6 \times {}^{15}NO_3^-$ assimilation/0.7.

We convert ^{14}C production estimates from 24 h incubations to gross C production by dividing by 0.65 to correct for dark respiration (assumed to equal 35% of gross production), and multiplying by 1.13 to correct for excretion of $DO^{14}C$

(as estimated by Bender et al., 1999). Hence, gross C production is $1.74 \times {}^{14}C$ production. We would derive a similar number using the rate terms in Laws et al. (2000b). We convert total ^{15}N production (defined as particulate uptake of $^{15}NO_3^- + {}^{15}NH_4^+ + {}^{15}N$-urea, when the latter is measured) to gross C production taking the Redfield C:N ratio of 6.6 and $DO^{15}N$ excretion as 30% of total ^{15}N assimilation. Hence, gross C production is $6.6 \times$ total ^{15}N assimilation/0.7, as for $^{15}NO_3^-$ assimilation. Finally, we scale gross O_2 production from $^{17}\Delta$ measurements to gross C production by accounting for the fraction of O_2 production linked to both the Mehler reaction and photorespiration, which is 20% of the measured O_2 production (here we follow Laws et al. (2000b), rather than Bender et al. (1999)). In our accounting, O_2 and C production that is consumed by photorespiration does not contribute to gross C production by definition. We assume that during O_2 cycling by the Mehler reaction, O_2 of $^{17}\Delta = 249$ per meg is produced, followed immediately by consumption of ambient O_2 (lower $^{17}\Delta$), without assimilation of C. Thus, $^{17}\Delta$ overestimates gross C production. We assume that the photosynthetic quotient for regenerated production is 1.1 (Laws, 1991). Hence, gross C production = net C production from $O_2 + (0.8 \times$ gross O_2 production–net O_2 production)/1.1.

4. Cruise locations and experimental methods

Surface water samples were collected: (a) on board the Nathaniel B. Palmer during December 1999, between 47°S and 68°S near 175°E; (b) on the same cruise in March 2000, along a route across the Bellingshausen Basin, from 70°S, 100°W to 65°S, 65°W, and then across the Drake Passage; and (c) aboard the Roger Revelle south of Australia, near 145°E in December 2000 and January 2001, between 45°S and 65°S during both the southbound and the northbound transits (Fig. 2).

We group the sample locations into four zones separated by three fronts of the Antarctic Circumpolar Current. The northern boundary of the Subantarctic Zone (SAZ) is the Subtropical Front

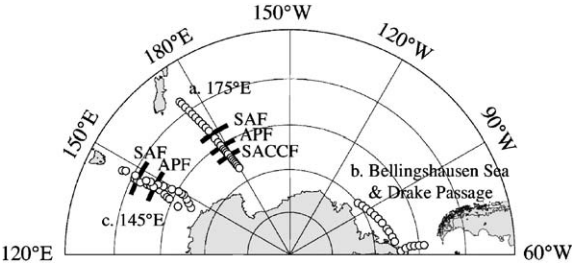

Fig. 2. Sample locations (a) South of New Zealand December 1999, 47–68°S, 174–180°E. (b) Eastern Bellingshausen Sea and Drake Passage March 2000, 70–65°S, 98–67°W and 64–58°S, 62–64°W. (c) South of Australia December 2000, 47.5–61.5°S, 147–143°E and January 2001, 64.5–48°S, 145–147°E. Map created with GMT software (www.aquarius.geomar.de/omc). Collection locations are marked with circles. Approximate locations of the fronts are shown by dark black bands.

and the southern boundary is the Subantarctic Front (SAF). The Subtropical Front lies north of our sample locations. The Polar Frontal Zone (PFZ) is bounded by the SAF to the north and the Antarctic Polar Front (APF) to the south. The Antarctic Zone (AZ) lies south of the APF and is bounded on the south by the Southern Antarctic Circumpolar Current Front (SACCF). The SACCF lies south of our sample locations at 145°E. The region south of the SACCF is called the "South of the Antarctic Circumpolar Current Zone" (SACCZ).

Frontal positions are marked by subsurface temperature and salinity gradients (Patterson and Whitworth, 1990). According to Pollard et al. (2002), the defining physical difference between the SAZ, PFZ and AZ is the relative contribution of temperature and salinity to stratification of the upper layer. In the northernmost zone, the SAZ, temperature controls stratification, while in the AZ salinity controls stratification. In the PFZ, temperature and salinity contribute about equally. Surface gradients in temperature and salinity also mark the frontal regions. We define the zonation on the basis of our surface temperature and salinity data (Fig. 3) following the definitions of Patterson and Whitworth (1990) and Belkin and Gordon (1996). The general locations of the three fronts, as we infer them (see Figs. 2 and 3), agree with Orsi et al. (1995) and Moore et al. (1999).

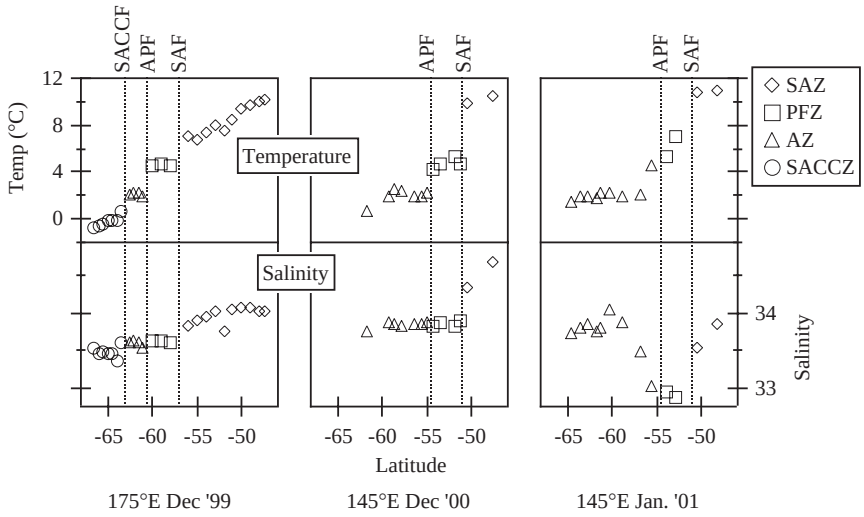

Fig. 3. Temperature (°C) and salinity data for the three crossings of the APF. Data from each cruise are divided into regions based on the locations of the SAF, APF and SACCF.

Along 175°E the SAF, APF and SACCF were characterized by three "steps" in the temperature and salinity data, which are obvious in the temperature data in Fig. 3. Between 57°S and 58°S there was a clear temperature drop from 7 to 4.5 °C, which marks the SAF. The APF is between 60°S and 61°S where the temperature changes from 4.5 to 2 °C. The SACCF is located between 62.5°S and 63.5°S where the temperature drops from 2 to 0.5 °C. Salinity changes in a similar step-like fashion at the SAF and the SACCF. The salinity gradient is not as pronounced at the APF. These locations and characteristics agree well with those from the December 1997 and January 1998 data from the Antarctic Environment and Southern Ocean Process Study (AESOPS) cruises (Smith et al., 2000; Sambrotto and Mace, 2000). To summarize, we mark the zones at 175°E as the SAZ (north of 57°S), the PFZ (57–60.5°S), the AZ (60.5–63°S), and the SACCZ (south of 63°S).

Along 145°E, the SAF was marked by a large temperature gradient, from 10 to 5 °C. This gradient appeared between 50.5°S and 51.5°S during December and between 51°S and 52°S in January. The APF displayed a similar temperature drop from 4 to 2 °C, between 54°S and 55°S in both December and January. The locations of these fronts are supported by the increased gradients in salinity at both fronts (except at the APF in December), the large north to south increase in surface $[NO_2^-]+[NO_3^-]$ and $[PO_4^{3-}]$ at the SAF, and the large north to south increase in silicate concentration at the APF (Sara Green, pers. comm.). The locations also agree with those of Rintoul et al. (1997). The zones at 145°E in December and January are as follows: the SAZ (north of 51°S), the PFZ (51–54.5°S), and the AZ (south of 54.5°S).

Temperature and salinity data for the cruise in the Bellingshausen Sea and the Drake Passage are shown in Fig. 4. We have broken the east–west transect of the Bellingshausen Sea into two sections at 78°W, based solely on productivity trends that are discussed later.

Approximately 150 ml of water was collected in 300 ml bottles that had been poisoned with 50 μl of saturated $HgCl_2$ solution (Kirkwood, 1992) and evacuated prior to the cruise. The bottles are constructed and filled as described in Emerson et al. (1995). The gases exsolve into the head space of the bottles and equilibrium is reached before the liquid is drained from the bottle without loss of the gases. The gas is prepared for mass spectrometric analysis of $\delta^{17}O$, $\delta^{18}O$, and $[O_2]/[Ar]$ according to

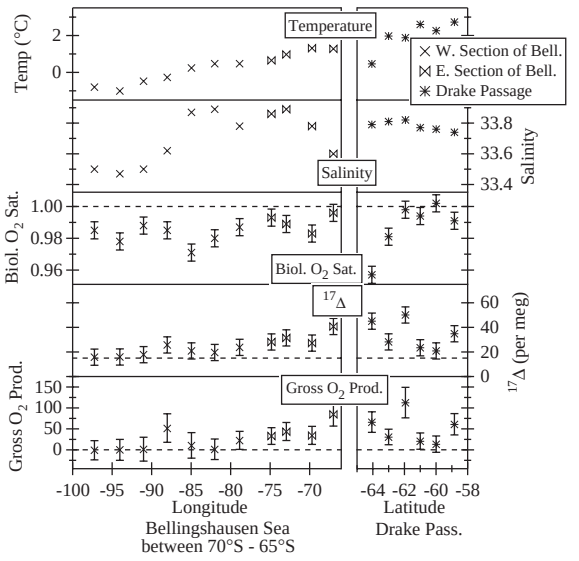

Fig. 4. Data for the Eastern Bellingshausen Sea and the Drake Passage. From top to bottom, the sections show temperature (°C), salinity, biological oxygen saturation, $^{17}\Delta$ (per meg), and gross O_2 production (mmol $O_2\,m^{-2}\,d^{-1}$). The section in the Bellingshausen Sea is broken into two groups based on the change in $^{17}\Delta$.

Blunier et al. (2002). Oxygen and argon are quantitatively separated from nitrogen in the sample by gas chromatography. The oxygen–argon mixture is expanded into the sample side of a Finnigan-Mat 252 isotope ratio mass spectrometer. Masses 32, 33 and 34 are measured against a standard mixture of oxygen and argon to determine $\delta^{17}O$ and $\delta^{18}O$. The O_2/Ar ratio in the sample is directly proportional to the ratio of mass 32 to mass 40, measured by single collector. The proportionality constant is determined by daily measurements of a compressed air standard. Each sample is analyzed for approximately 2 h to achieve high precision in the δ values.

We equate the uncertainty in our measurements with the pair-wise agreement of sample duplicates. Eighty-three pairs of samples were analyzed in this study. On average, replicates were measured 2.5 months apart. The mean of each pair and the deviation of each measurement from the mean were calculated. The standard deviation from the mean of these replicates was ± 9.4 per meg for $^{17}\Delta$ and ± 60 per meg for $\delta^{18}O$ (i.e. 68% of the replicates differed by less than 18.8 per meg for $^{17}\Delta$ and 120 per meg for $\delta^{18}O$). Mass spectrometry contributes ± 7.2 per meg (1σ) to the uncertainty in $^{17}\Delta$, based on variance in individual reference–sample–reference cycles. Sample handling, blank, and other sources contribute a similar amount, ± 6.0 per meg. The two numbers add in quadrature to ± 9.4 per meg. The overall uncertainty in $^{17}\Delta$ is thus far smaller than that for $\delta^{17}O$ or $\delta^{18}O$ alone. Most error in $\delta^{17}O$ and $\delta^{18}O$ is due to mass-dependent fractionation during sample processing, which has no effect on $^{17}\Delta$. For reference, the range of $^{17}\Delta_{dis}$ in this data set is 12–68 per meg and $\delta^{18}_{dis}O$ of the samples varies between 0‰ and 1‰.

Because the O_2/Ar ratio of each sample is determined by a single measurement of the $^{16}O_2$ and the ^{40}Ar mass spectrometer peaks, there is no measure of internal precision for the O_2/Ar measurements. We assess the overall error in these measurements by comparing agreement among all the compressed air measurements and the agreement between sample pairs. The standard deviation from the mean of the compressed air standards is $\pm 0.16\%$. Agreement between the samples is poorer. The standard deviation from the mean is $\pm 0.44\%$. There was a significant difference between the samples from the two cruises. As a group, the samples from 175°E were analyzed first, and the standard deviation from the mean was $\pm 0.54\%$. The standard deviation from the mean of the samples collected along 145°E was $\pm 0.21\%$. We attribute this difference to improved consistency in processing samples. We do not observe any change in O_2/Ar ratios with the length of time a bottle is stored before sampling. During the cruise along 145°E, 11 pairs of samples were collected from Niskin bottles, while the other 24 pairs of samples were collected sequentially from the ship's underway system. There is no systematic difference in precision, isotopic composition, or O_2/Ar of the samples collected by the different methods.

5. Biological oxygen saturation results

Biological oxygen saturation measurements for each transect of the APF are shown in Fig. 5. At

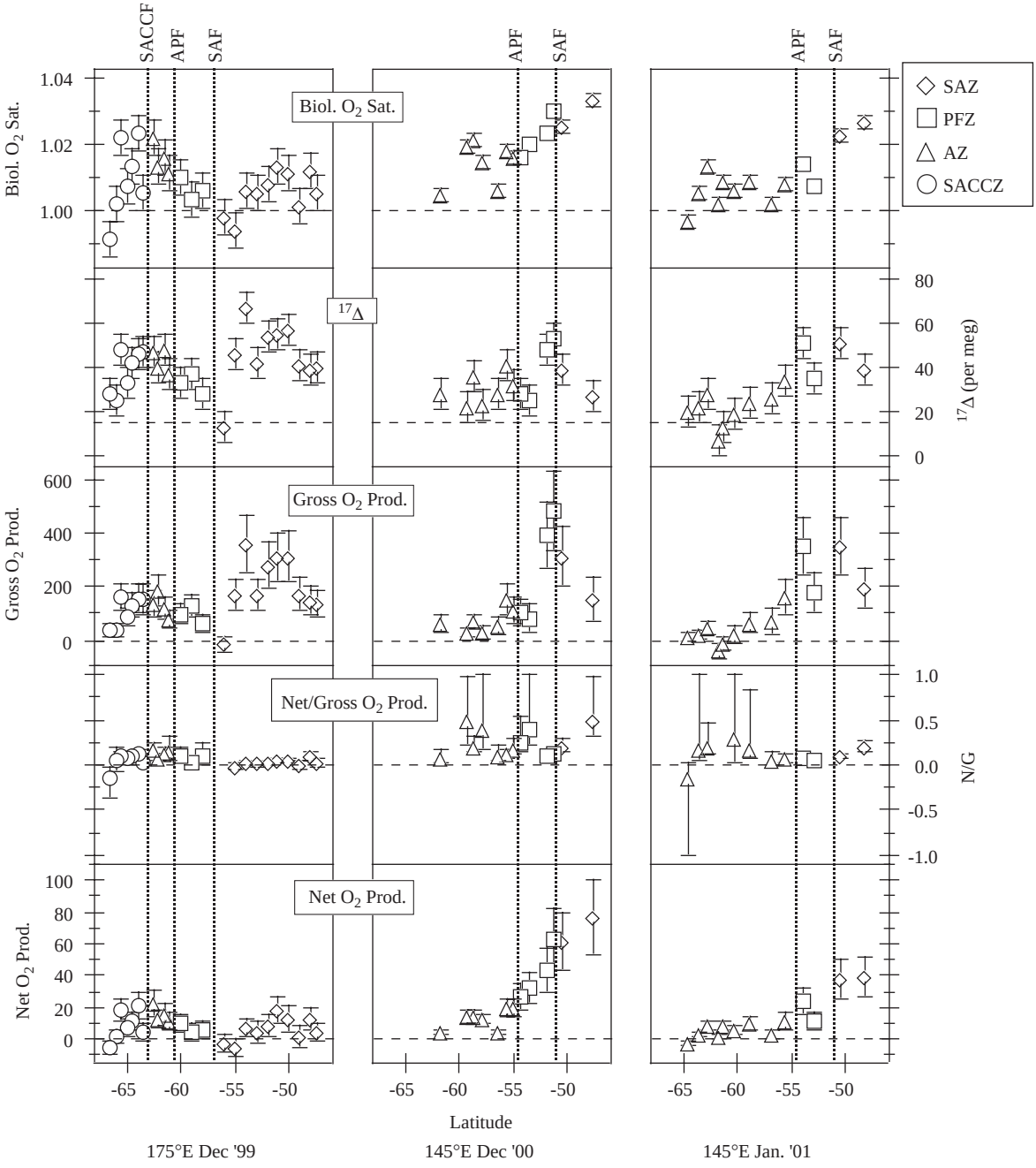

Fig. 5. Results based on measurements of biological oxygen saturation and triple oxygen isotope ratios for the three crossings of the APF. From top to bottom the sections show biological oxygen saturation, $^{17}\Delta$ (per meg), the rate of gross O_2 production (mmol $O_2\,m^{-2}\,d^{-1}$), the N/G O_2 production ratio, and the rate of net O_2 production (mmol $O_2\,m^{-2}\,d^{-1}$).

almost all locations, the biological oxygen saturation is greater than 1 (i.e. O_2 saturation, physical and biological, is greater than Ar saturation). The data from 175°E (left-most panel) and from 145°E (center and right-most panels) display different patterns in biological oxygen saturation. Along 175°E in December 1999, the biological oxygen saturation reaches a maximum near the SACCF, but shows no clear trend with latitude. In the SAZ, the biological oxygen saturation ranges from 99.5% to 101.5%. In the PFZ, AZ, and SACCZ, variability increases and the maximum measured biological oxygen saturation is almost 102.5%. Along 145°E, biological oxygen saturation decreases towards higher latitude, from ~103% in the north to ~100.5% near 62°S in December 2000. Biological O_2 saturation was about 1% lower in January 2001.

Biological O_2 supersaturations measured in this study at 175°E are much lower than O_2 supersaturations (physical and biological) measured in the region by Dickson and Orchardo (2001). They made continuous measurements of mixed layer O_2 concentrations across the APF during the US JGOFS Southern Ocean study near 170°W in December 1997, and calculated rates of net O_2 production with a gas exchange parameterization. Evidence for temporal variability comes from recent work of M. Reuer (Princeton University, pers. comm.), who has measured net production by a method identical to ours, and determined significantly higher rates.

Evidence for significant physical O_2 and Ar supersaturation comes from data collected on the 145°E cruise. During this cruise, C. Langdon (pers. comm.) measured $[O_2]$ by Winkler titration at our sample locations. We divide these values by our measured O_2/Ar ratios to determine absolute Ar concentrations. Ar concentrations are converted to Ar supersaturations based on temperature, salinity, and barometric pressure. The latter is based on NCEP reanalysis results for the individual study sites during the week prior to sampling. Using the equation for the saturation concentration from Weiss (1970), we find Ar supersaturations of $2.6 \pm 1.2\%$ ($n = 21$) at 145°E during December and January. Biological O_2 supersaturations (i.e. concentrations corrected for physical supersaturation) measured in this study are always $<3.3\%$ (Fig. 5), while total O_2 supersaturations measured by Dickson and Orchardo in December 1997 are $\leqslant 10\%$ (assuming an average saturation concentration of $300\,\mu mol\,l^{-1}$). Clearly, physical supersaturation contributes significantly to the total supersaturation, and net production calculated by Dickson and Orchardo (2001) represents an upper limit. The same is true for net O_2 production in the Ross Sea calculated by Bender et al. (2000). Agreement between net production rates estimated from measurements of $[O_2]$ and from O_2 incubations during the Bender et al. (2000) study support both values, but the closeness of agreement could be fortuitous because net O_2 production may be overestimated in 24 h incubations (Bender et al., 1999).

Fig. 4 shows the biological oxygen saturation for the samples from the Bellingshausen Sea and from the Drake Passage. With the possible exception of one location, biological oxygen saturation values are less than 1, by as much as 5%. There are two possible causes of undersaturation when samples are collected late in the growing season, as was done here. As the bloom wanes, the waters may become net heterotrophic. In addition, the mixed layer has begun to deepen by March, entraining underlying waters undersaturated in oxygen. We cannot distinguish between these explanations. Lacking a reliable model, we refrain from calculating net O_2 production for these samples.

6. $^{17}\Delta$ and gross O_2 production rates

Figs. 4 and 5 show the latitudinal distribution of $^{17}\Delta_{dis}$ (longitudinal distribution in the case of the Bellingshausen Sea). Values for $^{17}\Delta_{dis}$ range from $+12$ to $+68$ per meg, relative to atmospheric O_2. There are no obvious trends in $^{17}\Delta_{dis}$ with latitude across the APF along either 175°E or 145°E. Three points in the sections at 175°E and 145°E fall below the theoretical lower limit of 16 per meg (dashed line in Fig. 5). This is an expected consequence of analytical uncertainty. $^{17}\Delta_{dis}$ values in the Bellingshausen Sea are very low in the western part of the section. They increase to ~40

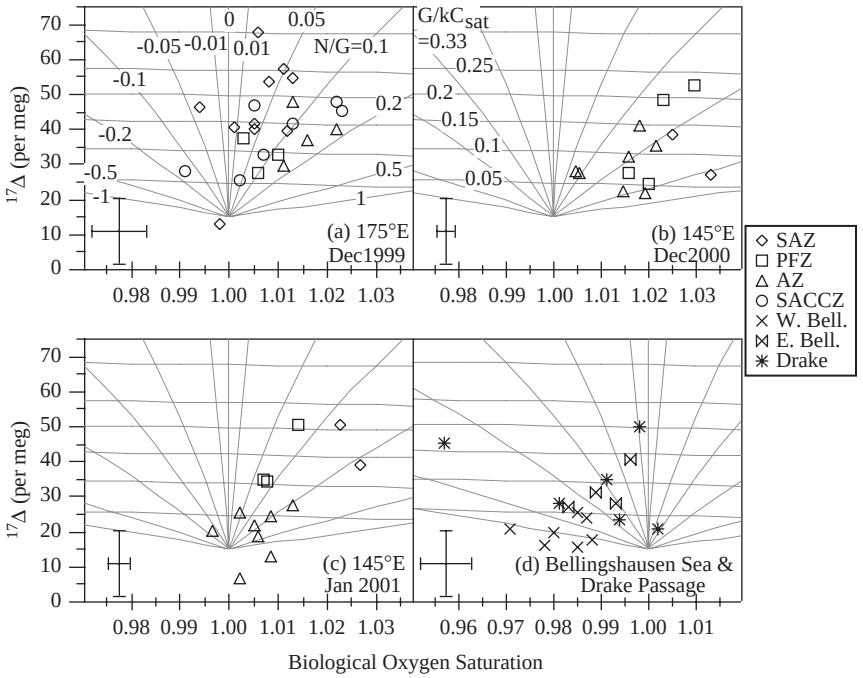

Fig. 6. $^{17}\Delta$ of dissolved O_2 (per meg) versus biological oxygen saturation at (a) 175°E, December 1999; (b) 145°E, December 2000; (c) 145°E, January 2001; and (d) the Bellingshausen Sea and the Drake Passage, March 2000. The subhorizontal lines are G/kC_{sat} isolines, labeled in panel (b). This term equals the ratio of the O_2 flux due to gross production divided by the O_2 flux into the ocean due to gas exchange. The lines that radiate from biol. O_2 sat. = 1 and $^{17}\Delta = 16$ are N/G O_2 production ratio isolines, labeled in (a). Representative error bars are shown for each group of samples.

per meg at the eastern end of the transect and are more variable (~20–50 per meg) in the Drake Passage.

Fig. 6 illustrates a graphical method for deriving G/kC_{sat} and N/G ratios from $^{17}\Delta_{dis}$ and biological O_2 saturation. In addition to the data, each panel has two sets of isolines, which apply to the steady-state mixed layer. The subhorizontal lines are isolines of constant G/kC_{sat}, based on Eqs. (2) and (5). The lines that radiate from the equilibrium point are isolines of constant N/G, based on Eqs. (3) and (5). Dissolved O_2 at equilibrium with the atmosphere has $C/C_{sat} = 1$ and $^{17}\Delta_{dis} = 16$ per meg (Luz and Barkan, 2000).

Sample G/kC_{sat} ratios in Fig. 6 range from less than 0 ($^{17}\Delta < 16$ per meg) to 0.33 ($^{17}\Delta \sim 65$ per meg). The three points below 16 per meg are assigned negative G/kC_{sat} values in proportion to their deviation from 16 per meg. C_{sat} values ranged from 274–367 mmol m^{-3}. Given gas exchange coefficients summarized in Section 2, the resulting rates of gross O_2 production were up to 500 mmol $m^{-2}\,d^{-1}$ (Fig. 5). Error bars in Fig. 5 are calculated assuming uncertainties of 6.6 per meg (standard error) for $^{17}\Delta$ replicate samples and 30% in the gas exchange rate (kC_{sat}).

The top panel of Fig. 7 shows the average gross O_2 production for each zone. The error bars are the standard deviation of the measurements and the number of data points in each average are indicated. All transects show a north to south trend of decreasing rates of gross O_2 production. Along 175°E, gross O_2 production is higher in the SAZ (avg = 203 ± 111 mmol $O_2\,m^{-2}\,d^{-1}$) than in the other zones, where the rates are comparable (95 ± 32, 130 ± 45, and 110 ± 55 mmol $O_2\,m^{-2}\,d^{-1}$ in the PFZ, AZ, and SACCZ, respectively). A similar north to south trend in gross O_2 production is obvious along 145°E, where the average rates in the SAZ (232 ± 110 and 273 ± 106, in

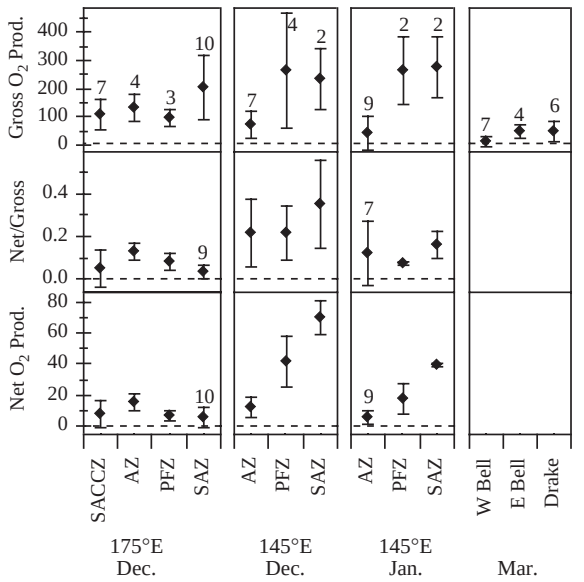

Fig. 7. Results averaged over each zone. From top to bottom: the rate of gross O_2 production (mmol $O_2\,m^{-2}\,d^{-1}$), the N/G ratio, and the rate of net O_2 production (mmol $O_2\,m^{-2}\,d^{-1}$). The error bars mark one standard deviation of the data and the numbers in the top panel denote the number of data points in each average. For reference, the analytical errors (see text) are comparable to the standard deviations of the fluxes. Fewer points were included in the averages of N/G in the SAZ at175°E in December and in the AZ at 145°E in January, as described in the text.

December and January, respectively) and PFZ (266 ± 203 and 265 ± 122 mmol $O_2\,m^{-2}\,d^{-1}$ in December and January, respectively) are much higher than the rates in the AZ (74 ± 46 and 39 ± 58 mmol $O_2\,m^{-2}\,d^{-1}$ in December and January, respectively). There is no obvious change in rates of gross O_2 production between December and January at 145°E.

The $^{17}\Delta_{dis}$ of samples collected in the Bellingshausen Sea and in the Drake Passage during March 2000 lie at the lower end of values measured on the other three transects (Figs. 4, 5 and 6). Even though the biological oxygen saturation in these samples is generally less than 1, $^{17}\Delta_{dis}$ of some samples is well above 16 per meg, indicating that photosynthetic oxygen is present in the dissolved O_2 pool. We assume that entrainment of O_2 undersaturated waters in March does not have a large impact on $^{17}\Delta_{dis}$ because [O_2] of the entrained waters is low, and $^{17}\Delta$ of the added O_2 is probably not far from the equilibrium value of 16 per meg. Since our model of the mixed layer does not recognize incorporation of low $^{17}\Delta_{dis}$ waters from below the mixed layer, our estimates of gross O_2 production in the Bellingshausen Sea and the Drake Passage are lower limits. It is also possible, but unlikely, that waters below the mixed layer have $^{17}\Delta_{dis} > 16$ per meg. At the BATS Station, a $^{17}\Delta_{dis}$ maximum is produced in the thermocline (Luz and Barkan, 2000). However, summer-time thermocline waters in the Southern Ocean are ventilated in the deep, winter-time mixed layer, which would have little, if any photosynthetic O_2. Furthermore, many of our undersaturated samples are close to $^{17}\Delta_{dis} = 16$ per meg (e.g. the Western section of the Bellingshausen Sea in Fig. 4).

Rates of gross O_2 production in March are very low (12 ± 19, 49 ± 24, and 50 ± 37 mmol $O_2\,m^{-2}\,d^{-1}$ west of 78°W, east of 78°W, and in the Drake Passage, respectively), comparable to the rates of gross O_2 production found in the AZ at 145°E (Fig. 7). At all but one of the sites west of 78°W, the rate of gross O_2 production is within error of zero.

7. N/G ratios and net O_2 production rates

According to the position of each data point in Fig. 6 we assign an N/G ratio (Fig. 5). The three points that fall below $^{17}\Delta = 16$ per meg are assigned undefined N/G ratios. These points are excluded from Fig. 5 and from calculations of regional averages in Fig. 7. Error limits on N/G ratios were calculated assuming uncertainties in biological O_2 saturation and $^{17}\Delta$ as described in Section 4. N/G ratios outside the range of $-\infty$ to $+1$ are theoretically impossible in the $^{17}\Delta$ method and error bars are limited to this range. Net O_2 production is calculated from Eq. 9. Errors are calculated based on the uncertainties in biological O_2 saturation in Section 4 and an uncertainty of 30% in the gas exchange rate, kC_{sat}.

Along 175°E in December, all N/G ratios are less than 0.2 (Figs. 5 and 6). Fig. 7 shows that the average N/G is lowest in the SAZ (0.03 ± 0.03)

and the SACCZ (0.05 ± 0.09). N/G approximately doubles in the PFZ (0.08 ± 0.04) and triples in the AZ (0.13 ± 0.04). For all samples along 175°E in December 1999, the average N/G was 0.06 ± 0.07.

N/G ratios are higher at 145°E than at 175°E in both December 2000 (overall average = 0.24 ± 0.15) and in January 2001 (overall average = 0.11 ± 0.12). Comparison of the regional N/G averages during December at 145°E in Fig. 7 shows no clear difference between the zones ($N/G = 0.35 \pm 0.21$, 0.22 ± 0.13, and 0.22 ± 0.16 in the SAZ, PFZ, and AZ, respectively). Again in January, there was no obvious trend in N/G ratios (0.16 ± 0.06, 0.07 ± 0.01, and 0.12 ± 0.15 in the SAZ, PFZ, and AZ, respectively), but the overall average had decreased by 50% from the previous month. It remains to be seen whether the spatial difference observed between 175°E and 145°E or the temporal difference between December and January at 145°E are maintained from year to year.

Overall, net production ranged from ~ -5 to 75 mmol $O_2\,m^{-2}\,d^{-1}$ (Fig. 5). Our net production data show three trends. First, net production at 145°E in December (30 ± 24 mmol $O_2\,m^{-2}\,d^{-1}$) and in January (13 ± 13 mmol $O_2\,m^{-2}\,d^{-1}$) is higher than net production in December at 175°E (8 ± 8 mmol $O_2\,m^{-2}\,d^{-1}$). Second, net production at 145°E was higher in December than in January. Third, at 145°E, net production decreased poleward during both December and January. December rates were 70 ± 11, 41 ± 16, 13 ± 6 mmol $O_2\,m^{-2}\,d^{-1}$ in the SAZ, PFZ, and AZ, respectively. Equivalent rates in January were 39 ± 1, 18 ± 10, 6 ± 4 mmol $O_2\,m^{-2}\,d^{-1}$. No clear meridional trend is observed in December at 175°E.

8. Comparisons with other data and a model prediction

To compare our rates of O_2 production to other measurements made in the same regions of the Southern Ocean, we convert all measurements to rates of C production, as described in Section 3 (Table 1). The US JGOFS Southern Ocean Study, also known as AESOPS, studied biogeochemical fluxes along 170°W and provides the most detailed comparison (Smith et al., 2000). Even though our study and AESOPS were not carried out at the same time, a comparison of the results is useful until a full complement of simultaneous measurements, including the triple isotope technique, is performed. ^{15}N incubations were performed by Sambrotto and Mace (2000) during both transects of the APF to determine ^{15}N *f*-ratios as well as rates of new and total production. Other data sets from the APF transect provide estimates of net C production. Buesseler et al. (2001) estimate export of particulate organic C from ^{234}Th fluxes at various depths between 5 and 300 m. As part of the compilation of Nelson et al. (2002), average seasonal net production was estimated from NO_3^- drawdown over the growing season. Morrison et al. (2001) estimated net C production based on the seasonal change in pCO_2. We do not include O_2 and ^{14}C incubation data from the JGOFS AESOPS program because of the mismatch between in situ and incubator irradiance (Dickson and Orchardo, 2001).

As in our study, sample groupings in the AESOPS study are based on the locations of the fronts; however, they differ from our categories in two ways. First, a new region, the APF region, is added at the PF that encompasses the southern part of the PFZ and the northern part of the AZ. Second, the northern edge of the SACCZ at 170°W is farther south than in our study at 175°E, significantly decreasing the size of this zone. The sample locations of AESOPS are grouped in the following manner: the SAZ, 47–55°S; the zone north of the APF (NAPF, 55–59°S); the APF region (APFR, 59–61.5°S); the zone south of the APF (SAPF, 61.5–65.5°S); and the zone south of the ACC (SACCZ, 65.5–68°S). (See Fig. 1 of Buesseler et al. (2001).) Because results for the AESOPS studies are already published according to these groupings, we regroup all of our samples along 175°E in the same manner to facilitate comparisons (Table 1).

The data for comparisons in the second region of the Southern Ocean come from several cruises in the SAZ and PFZ south of Australia. Elskens et al. (2002) determined ^{15}N *f*-ratios from uptake rates of $^{15}NO_3^-$, $^{15}NH_4^+$, and ^{15}N-labeled urea in incubation studies along 142°E, between 42°S and

Table 1
Estimates of Southern Ocean production

145°E						175°E–170°W								
		O_2, $^{17}\Delta$ (1)		^{15}N (2)	NO_3^- (3)			O_2, $^{17}\Delta$ (1)	^{15}N (4)		^{234}Th (5)		NO_3^- (6)	pCO_2 (7)
		Dec	Jan	Mar	Seas			Dec	Dec	Feb	Dec	Feb	Seas	Seas
Gross C production (mmol C m^{-2} d^{-1})														
SAZ	47–51°S	155	191			SAZ	47–55°S	164						
PFZ	51–55°S	185	189			NAPF	55–59°S	18	298	224				
						APFR	59–61.5°S	71	327	83				
AZ	55–65°S	51	27			SAPF	61.5–65.5°S	98	335	264				
						SACCZ	65.5–68°S	57						
Net/gross C production														
SAZ	47–51°S	0.39	0.16	0.34		SAZ	47–55°S	0.03						
PFZ	51–55°S	0.24	0.06	0.43		NAPF	55–59°S	0.13	0.08	0.08				
						APFR	59–61.5°S	0.09	0.20	0.20				
AZ	55–65°S	0.24	0.02	0.33		SAPF	61.5–65.5°S	0.10	0.21	0.09				
						SACCZ	65.5–68°S	0.01						
Net C production (mmol C m^{-2} d^{-1})														
SAZ	47–51°S	50	28		28	SAZ	47–55°S	5			11	9		
PFZ	51–55°S	29	13		12	NAPF	55–59°S	2	24	18	6	16	18	25
						APFR	59–61.5°S	6	65	17	14	12	22	28
AZ	55–65°S	9	4			SAPF	61.5–65.5°S	10	70	24	11	12	27	30
						SACCZ	65.5–68°S	3				19	14	37

All measurements have been converted to C production (mmol C m^{-2} d^{-1}) by the methods outlined in the text.
Citations: (1) $^{17}\Delta$ of dissolved O_2 (this study); (2) ^{15}N incubations (Elskens et al., 2002); (3) seasonal drawdown of NO_3^- (Lourey and Trull, 2002); (4) ^{15}N incubations (Sambrotto and Mace, 2000); (5) ^{234}Th fluxes at various depths (Buesseler et al., 2001); (6) seasonal drawdown of NO_3^- (Nelson et al., 2002); and (7) seasonal drawdown of pCO_2 (Morrison et al., 2001).

56°S during March 1998. Lourey and Trull (2002) estimated net C production from measurements of NO_3^- depletions between a July section of the World Ocean Circulation Experiment (SR3) and eight additional sections between October and March during the years 1991–1998. Sample groupings along 145°E remain the same: the SAZ, north of 51°S; the PFZ, 51–54.5°S; and the AZ, south of 54.5°S.

A number of patterns emerge from the comparisons of our data from 175°E collected in December and those of AESOPS at 170°W (Table 1). Gross and net C production rates measured with ^{15}N are far greater than rates measured in this study. C export rates measured with ^{234}Th are intermediate, but closer to our net C production rates measured with O_2.

Comparisons between our measurements of net production from O_2 and net production estimated from both the seasonal NO_3^- drawdown (Nelson et al., 2002; Lourey and Trull, 2002) and the pCO_2 change (Morrison et al., 2001) are complicated by temporal and spatial variability. Our data reflect production during ~10 days prior to sampling, while drawdown estimates integrate through the entire growing season. Net production may change as the bloom evolves. The limited results of this study suggest this is the case at 145°E as the rates of net production decrease between December and January. In addition, water sampled for drawdown estimates along most of the AESOPS line during the middle and end of summer was further to the southwest earlier in the growing season.

This discussion suggests that perhaps the best approach to minimize the effect of our shorter integration time and smaller spatial footprint is to combine our estimates from 145°E and 175°E for comparison with the inventory data at 145°E and

170°W. The average net production from our measurements in the PFZ at 145°E and the NAPF at 175°E is 15 mmol C $m^{-2} d^{-1}$ (= avg. of 29, 13, and 2 mmol C $m^{-2} d^{-1}$). This compares well with the average of the inventory drawdown estimates in the PFZ at 145°E and the NAPF at 170°W, 18 mmol C $m^{-2} d^{-1}$ (= avg. of 12, 18, and 25 mmol C $m^{-2} d^{-1}$). However, our average value of net production in the AZ at 145°E and the SAPF at 175°E, 8 mmol C $m^{-2} d^{-1}$, (= avg. of 9, 4, and 10 mmol C $m^{-2} d^{-1}$) is much lower than the average inventory estimate in the SAPF at 170°W, 28 mmol C $m^{-2} d^{-1}$ (= avg. of 27 and 30 mmol C $m^{-2} d^{-1}$: no inventory estimate is available in the AZ at 145°E).

N/G C production ratios determined in this study from O_2 properties differ considerably from ^{15}N *f*-ratios (Table 1). At 175°E and 170°W, ^{15}N *f*-ratios and *N/G* ratios are comparable in the NAPF, but ^{15}N *f*-ratios are higher by a factor of 2 in the APFR and SAPF. At 145°E, ^{15}N *f*-ratios measured in March are again higher than *N/G* ratios measured in December and January from O_2 properties.

Overall, the comparison can be summarized as follows. C production rates and *f*-ratios measured with ^{15}N are generally much higher than values based on O_2 properties. Net C production rates constrained with O_2 properties agree reasonably well with C export rates measured using ^{234}Th. They also fall within the range of net C production rates estimated from seasonal inventory changes in the PFZ, but are much lower to the south.

The pelagic food web model of Laws et al. (2000a) fits a series of observations and predicts a strong inverse relationship between local temperature and *ef*-ratios (new, net or export C production/gross or total C production) on a global scale. However, over the temperature range typical of the Southern Ocean, 0–10 °C, the model predicts that *ef*-ratios vary little with temperature, but rather depend on the rate of gross production. High *ef*-ratios (~0.5–0.7) are predicted in regions of moderate to high rates of gross C production (>200 mmol C $m^{-2} d^{-1}$), and there is a steep transition to low *ef*-ratios (<0.2) at very low production rates (Fig. 8, see also Fig. 2 of Laws et al., 2000a).

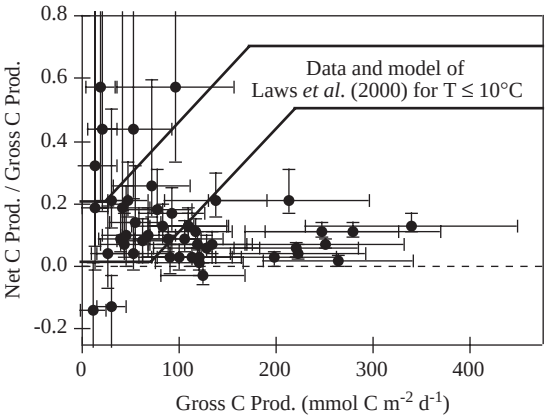

Fig. 8. Net/gross C production ratios from this study and *ef*-ratios based on the model prediction of Laws et al. (2000a). Our *N/G* values differ slightly from those in Fig. 4, because they have been converted from rates of O_2 production to rates of *C* production. The zone outlined in black is our estimate of the model *ef*-ratios over the temperature range 0–10 °C, based on Fig. 2 of Laws et al. (2000a). Total N production (mg N $m^{-3} d^{-1}$) of Laws et al. (2000a) is converted to gross C production (mmol C $m^{-2} d^{-1}$) assuming a mixed layer depth of 50 m and a molar Redfield C:N ratio of 6.6.

Our values for the ratios of net to gross C production are consistently low (regional means of 0–0.4, Fig. 7), which generally agree with the model results in the Southern Ocean (Plate 3; Laws et al., 2000a). However, our results do not indicate an increase in *N/G* ratios with increased gross production, as the model predicts (Fig. 8). At low gross production rates, we observe low *N/G* ratios as predicted by Laws et al. (2000a). All of the high *N/G* ratios agree with Laws et al. (2000a) within the large uncertainties of these samples. At higher rates of gross production (>200 mmol C $m^{-2} d^{-1}$), our *N/G* ratios are well below the model of Laws et al. (2000a) and its supporting data (Fig. 8).

All of the above intercomparisons are problematic. Comparison values were measured during different years, different times of the year, and somewhat different locations. As noted above, net production and *N/G* ratios, measured in a subsequent study by M. Reuer (pers. comm.) using identical techniques, are higher than values reported here. All methods of constraining metabolic rates have important uncertainties and significant limitations. Bottles may selectively

sample the biota, and enclose communities under conditions differing from those in situ. ^{234}Th fluxes entail assumptions about C/^{234}Th ratios. Inventory approaches examine seasonal changes in water chemistry but cannot take into account the fact that water present at the end of the growing season was in a different location at the beginning of the growing season. Rates reported here based on O_2 properties have large analytical uncertainties, and use gas exchange parameterizations that are uncertain. Our measurements also constrain rates to the bottom of the mixed layer, and these may differ significantly from rates integrated to the base of the euphotic zone. The intercomparison of methods is critical, and ultimately this work must be performed on expeditions where conditions are well defined and multiple approaches can be applied in the same waters.

Specifically addressing the results of Laws et al. (2000a), there are two neglected conditions that could lead us to underestimate N/G C production in our steady-state model. The first is that photosynthetic production and respiration may not be at steady state. The O_2 properties of the mixed layer reflect conditions over the past ~10 days, and one could imagine that they have varied systematically in a way that suggests N/G values that are not representative. It seems unlikely that this was a chronic condition during our cruises: the bloom begins well before our sampling and SeaWiFS data show that chlorophyll does not change much between November, December, and January (seawifs.gsfc.nasa.gov/SEAWIFS.html). Our samples were collected during the latter two months.

Another possible cause of low N/G C production ratios is entrainment of O_2 undersaturated waters from below the mixed layer. To evaluate this possibility, we examined depth profiles of O_2 in the upper water column during Kiwi Leg 7 (December, 1997) of the US JGOFS Southern Ocean Program (www1.whoi.edu/jgofs.html). At most stations, waters below the mixed layer had O_2 supersaturations comparable to those in the mixed layer, suggesting that entrainment would not systematically bias O_2 supersaturations to low values.

9. $\delta^{18}O$ Results

Fig. 9a plots $\delta^{18}_{dis}O$ versus biological oxygen saturation from our mixed layer samples. $\delta^{18}_{dis}O$ increases as biological oxygen saturation decreases. When biological O_2 saturation ~ 1.03, $\delta^{18}_{dis}O$~ 0.1‰. $\delta^{18}_{dis}O$ rises to ~ 0.85‰ when biological saturation falls to 0.97. (At equilibrium, $\delta^{18}_{dis}O$ ~ +0.8‰.) This trend is consistent with results of surface and subsurface samples at other locations (Quay et al., 1993; Kroopnick and Craig, 1976; Bender and Grande, 1987; Bender et al., 2000). At biological oxygen saturation of 1, $\delta^{18}_{dis}O$ of the samples is approximately 0.2–0.4‰ less than the atmospheric equilibrium point because of the addition of photosynthetic O_2 ($\delta^{18}O = -22.96$‰). Quay et al. (1993) found similar values for $\delta^{18}_{dis}O$ of surface samples in the subarctic Pacific. In the Ross Sea, during summer and fall 1997, the displacement from equilibrium was greater;

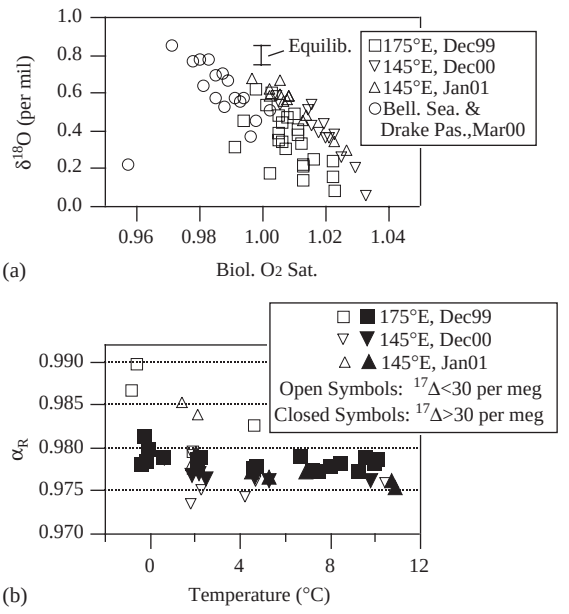

Fig. 9. (a) $\delta^{18}_{dis}O$ of all samples versus biological oxygen saturation. (b) α^{18}_R versus local temperature. The open symbols correspond to samples of $^{17}\Delta < 30$ per meg. At these low values of $^{17}\Delta$, N/G is not well constrained and the resulting values for α^{18}_R are more uncertain. The closed symbols correspond to samples where $^{17}\Delta > 30$ per meg. The average α^{18}_R of the closed symbols is 0.978 ± 0.001.

$\delta^{18}_{dis}O \sim -2‰$ ($\sim$2.8‰ below equilibrium) at $[O_2]$ saturation (Bender et al., 2000). This lower $\delta^{18}_{dis}O$ agrees qualitatively with the higher rates of gross production found in that study.

From Eq. (3), the N/G ratio can theoretically be determined from measurements of the biological oxygen saturation and $\delta^{18}_{dis}O$, without reliance on $^{17}\Delta_{dis}$. The main shortcoming of this method, discussed above, is the uncertainty in α^{18}_R. One can reverse the situation and calculate α^{18}_R knowing N/G. Quay et al. (1993) calculated α^{18}_R of 0.978 ± 0.006 for the collective marine community in the mixed layer from observations of the changes in $[O_2]$ and $\delta^{18}_{dis}O$ in the surface waters of the subarctic Pacific. The large error reflects uncertainties in upper ocean O_2 fluxes and mixing dynamics. Below the mixed layer (100–280 m), Quay et al. (1993) calculated a higher fractionation factor, 0.980–0.988. Bender (1990) estimated α^{18}_R as 0.982 in the deep ocean. Euphotic zone and aphotic zone values are not necessarily the same since the ecological community structure differs between the two regions. Guy et al. (1993) and Kiddon et al. (1993) measured α^{18}_R values ranging from 0.975 to 0.985 for various organisms in laboratory experiments.

We use the measured $\delta^{18}_{dis}O$ and biological oxygen saturation, along with the calculated values of N/G, to solve Eq. (3) for α^{18}_R. This is a reliable approach since determination of N/G ratios from $^{17}\Delta_{dis}$ measurements is practically insensitive to the exact value of α^{18}_R. It depends, instead, on the ratio of $\ln \alpha^{17}_R$ to $\ln \alpha^{18}_R$, which we know accurately. Fig. 9b shows the results of these calculations for samples collected along 175°E and 145°E. Measurements from the Bellingshausen Sea and the Drake Passage are not included because we cannot calculate N/G for those samples. There is no obvious trend in α^{18}_R with temperature or latitude. Samples where $^{17}\Delta_{dis}$ is less than 30 per meg are distinguished from the other samples. The uncertainty in the N/G and G/kC_{sat} ratios in these low $^{17}\Delta_{dis}$ samples is relatively large since the isolines are very close to each other (see Fig. 6). The average of all the values of α^{18}_R is 0.978 ± 0.003 ($n = 47$), equivalent to an isotope effect, ε^{18}_R, of $-22 \pm 3‰$. When including only those points where $^{17}\Delta_{dis}$ is greater than 30 per meg, we calculate an isotope effect of $-22 \pm 1‰$ ($\alpha^{18}_R = 0.978 \pm 0.001$: $n = 30$). These results agree well with Quay et al. (1993), and are compatible with other upper ocean data (Bender and Grande, 1987; Bender et al., 2000). It is notable that this high isotope effect would help explain the Dole effect of $+23.5‰$, which is the $\delta^{18}O$ of atmospheric O_2 with respect to mean ocean H_2O (Lane and Dole, 1956; Kroopnick and Craig, 1972; Bender et al., 1994).

10. Conclusions

In this paper, we apply the triple isotope method first implemented by Luz and Barkan (2000), to constrain net production, gross production, and net/gross production ratios in the mixed layer of the Southern Ocean. This method should become a standard technique applied during ecosystem studies. Results for our three summertime transects suggest significant spatial and seasonal variability in net and gross production rates. Nevertheless, we can make some generalizations. On each transit, gross production rates are higher in the north than in the south. On two of the three transits, net production rates also decreased from north to south. Net and gross production rates determined in this study agree with values in some independent data sets and disagree with others. Net/gross C production ratios are low (generally <0.2) at all locations, including regions of high gross C production (200–450 mmol $C\,m^{-2}\,d^{-1}$). Methodological issues need to be investigated by making simultaneous measurements using the concentration and isotopic composition of O_2 along with other approaches.

Acknowledgements

We wish to thank Stan Jacobs, Suzanne O'Hara, and Sara Green for collecting these samples, and Chris Langdon for sharing results of Winkler titrations from the cruise along 145°E. We very much appreciate work on the analysis method and many discussions by Thomas Blunier, Boaz Luz, and Matthew Reuer. This work was supported by grants from NASA and NSF.

Appendix

Here we derive the formal equations and approximations described in Section 2. We assume that there is no mixing across the base of the mixed layer. We also neglect the small influence of physical supersaturation (due to warming and bubble injection) on $\delta^{17}O$ and $\delta^{18}O$ of dissolved O_2.

Eq. (1), repeated here from the main text, describes the steady-state O_2 concentration integrated over the depth of the mixed layer after correcting for, or neglecting, physical supersaturation (Emerson, 1987).

$$h\frac{dC}{dt} = 0 = G - R + k(C_{sat} - C). \quad (1)$$

This equation applies to each of the three isotopic species of interest ($^{16}O_2$, $^{17}O^{16}O$, $^{18}O^{16}O$). Eq. (A.1) is the steady-state condition for $^{17}O^{16}O$ and $^{18}O^{16}O$, analogous to Eq. (1). (We assume that Eq. (1) applies to $^{16}O_2$ as it is written.)

$$h\frac{d}{dt}\left(CX^*_{dis}\right) = 0 = GX^*_W\alpha^*_P - RX^*_{dis}\alpha^*_R + kC_{sat}X^*_{sat} - kCX^*_{dis}. \quad (A.1)$$

The product CX^*_{dis} is the concentration of the isotopomer (mmol $^{18}O^{16}O$ or $^{17}O^{16}O$ m^{-3}) dissolved in the mixed layer. X^*_W is the isotopic ratio of oxygen in seawater (H_2O). Since there is no fractionation of oxygen isotopes associated with conversion of H_2O to O_2 by photosynthesis, α^*_P, the fractionation factor associated with photosynthesis, is equal to 1 (Guy et al., 1993) and it drops out of the equation. α^*_R is the fractionation factor for respiration. X^*_{sat} is the isotopic ratio of dissolved O_2 that is in equilibrium with the atmosphere. We neglect the small isotopic fractionation associated with gas exchange.

We substitute $G + k(C_{sat} - - - C)$ in Eq. (A.1) for R and divide each side by the isotopic ratio of the standard, X^*_{std}, which is atmospheric O_2. Then we can write an equation for $\delta^*_{dis}O$ in terms of G/kC, C/C_{sat}, and α^*_R.

$$\delta^*_{dis}O/10^3 = \frac{(G/kC_{sat})(\delta^*_W O/10^3 + 1) + (\delta^*_{sat}O/10^3 + 1)}{(G/kC_{sat}) + 1 - ((G/kC_{sat}) + 1 - (C/C_{sat}))(1 - \alpha^*_R)} - 1, \quad (2)$$

$\delta^*_{dis}O$ can also be written in terms of N/G, C/C_{sat}, and α^*_R.

$$\delta^*_{dis}O/10^3 = \frac{(C/C_{sat} - 1)(\delta^*_W O/10^3 + 1) + (N/G)(\delta^*_{sat}O/10^3 + 1)}{(C/C_{sat}) - 1 + (N/G) - (1 - (N/G))((C/C_{sat}) - 1)(1 - \alpha^*_R)} - 1. \quad (3)$$

Formal expressions for $^{17}\Delta_{dis}$ in terms of G/kC_{sat} and C/C_{sat} and in terms of N/G and C/C_{sat} follow by substitution of Eqs. (2) and (3), respectively, in the definition $^{17}\Delta/10^6 = \ln(\delta^{17}O/10^3 + 1) - 0.516\ln(\delta^{18}O/10^3 + 1)$. The G/kC_{sat} isolines in Fig. 6 come from substitution of Eq. (2) in the definition of $^{17}\Delta$. N/G isolines in Fig. 6 are the result of substitution of Eq. (3) in the definition of $^{17}\Delta$. In our calculations and in Fig. 6, we use the following values for the isotopic ratios and the fractionation factors. Kroopnick and Craig (1972) report $\delta^{18}O$ of atmospheric O_2 with respect to SMOW, i.e. $(X^{18}_{atm}/X^{18}_{SMOW} - 1) \times 10^3$, as +23.5‰. After this value is converted to $\delta^{18}O$ of SMOW with respect to atmospheric O_2, i.e. $(X^{18}_{SMOW}/X^{18}_{atm} - 1) \times 10^3$, we have $\delta^{18}_W O = -22.960$‰. $^{17}\Delta_W$ from Luz and Barkan (2000) is 249 per meg. Then from the definition of $^{17}\Delta$, $\delta^{17}_W O = -11.668$‰. $\delta^{18}_{sat}O$ is close to 0.8‰ at the surface temperatures of the Southern Ocean (exact values are given by Benson and Krause, 1984) and $^{17}\Delta_{sat}$ is 16 per meg (Luz and Barkan, 2000). We use these values to calculate a $\delta^{17}_{sat}O$ value of 0.429‰. We take α^{18}_R as 0.982 (Bender, 1990; Kiddon et al., 1993) and α^{17}_R as 0.99067; this value for the ^{17}O fractionation factor is compatible with the coefficient of 0.516 in Eq. (4).

To demonstrate the utility of $^{17}\Delta$ and derive the equations in the main text we use the approximate form, $^{17}\Delta/10^6 \approx \Delta^{17}O/10^6 = \delta^{17}O/10^3 - 0.516 \cdot \delta^{18}O/10^3$. We can use this simplification because $\delta^{17}O$ and $\delta^{18}O$ of all the samples and dissolved O_2 at equilibrium are within 0–1‰. We return to

Eq. (A.1), and solve for $\delta^*_{dis}O$, without eliminating R from the expression.

$$\delta^*_{dis}O/10^3 = \frac{G\delta^*_W O/10^3 + kC_{sat}\delta^*_{sat}O/10^3 + R(1-\alpha^*_R)}{G + kC_{sat} - R(1-\alpha^*_R)}. \quad (A.2)$$

The first term in the denominator is much less than the second. The third term can be ignored as it is much smaller than the first. This is because $R \sim G$ when the mixed layer is at steady state, and α^*_R is close to 1. The same term in the numerator cannot be neglected because $\delta^*_W O/10^3$ and $\delta^*_{sat}O/10^3$ are of the same order as $1-\alpha^*_R$.

Neglecting the respiration term in the denominator of Eq. (A.2), the expression for $\Delta^{17}O_{dis}$ is as follows:

$$\Delta^{17}O_{dis}/10^6 = \frac{G\delta^{17}_W O/10^3 + kC_{sat}\delta^{17}_{sat}O/10^3 + R(1-\alpha^{17}_R)}{G + kC_{sat}} - 0.516\frac{G\delta^{18}_W O/10^3 + kC_{sat}\delta^{18}_{sat}O/10^3 + R(1-\alpha^{18}_R)}{G + kC_{sat}}. \quad (A.3)$$

We can simplify this expression by removing the respiration terms; this simplification is possible because $(1-\alpha^{17}_R) \approx 0.516(1-\alpha^{18}_R)$. Use of this approximation makes a difference in $\Delta^{17}O_{dis}$ of less than 3 per meg for typical conditions of the mixed layer.

Then our final expression for $\Delta^{17}O_{dis}$, as shown in the main text, is

$$\Delta^{17}O_{dis} = \frac{(G/kC_{sat})\Delta^{17}O_W + \Delta^{17}O_{sat}}{(G/kC_{sat}) + 1},$$
$$\frac{G}{kC_{sat}} = \frac{\Delta^{17}O_{sat} - \Delta^{17}O_{dis}}{\Delta^{17}O_{dis} - \Delta^{17}O_W}. \quad (7)$$

An expression for $\Delta^{17}O_{dis}$ in terms of N/G and C/C_{sat} results from substitution of $N/(C-C_{sat})$ for k (see Eq. (9)).

$$\Delta^{17}O_{dis} = \frac{(C/C_{sat}-1)\Delta^{17}O_W + (N/G\Delta^{17}O_{sat})}{C/C_{sat} - 1 + N/G},$$
$$\frac{N}{G} = \left(\frac{C}{C_{sat}} - 1\right)\frac{\Delta^{17}O_{dis} - \Delta^{17}O_W}{\Delta^{17}O_{sat} - \Delta^{17}O_{dis}}. \quad (8)$$

References

Angert, A., Rachmilevitch, S., Barkan, E., Luz, B., 2003. Effects of photorespiration, the cytochrome pathway, and the alternative pathway on the triple isotopic composition of atmospheric O_2. Global Biogeochemical Cycles 17 (1), doi:10.1029/2002GB001933.

Arrigo, K.R., Worthen, D., Schnell, A., Lizotte, M.P., 1998. Primary production in Southern Ocean waters. Journal of Geophysical Research—Oceans 103 (C8), 15587–15600.

Belkin, I.M., Gordon, A.L., 1996. Southern Ocean fronts from the Greenwich meridian to Tasmania. Journal of Geophysical Research—Oceans 101 (C2), 3675–3696.

Bender, M.L., 1990. The delta-O-18 of dissolved O2 in seawater—a unique tracer of circulation and respiration in the deep-sea. Journal of Geophysical Research—Oceans 95 (C12), 22243–22252.

Bender, M.L., 2000. Oceanography—tracer from the sky. Science 288 (5473), 1977–1978.

Bender, M.L., Grande, K.D., 1987. Production, respiration, and the isotope geochemistry of O_2 in the upper water column. Global Biogeochemical Cycles 1, 49–59.

Bender, M.L., Sowers, T., Labeyrie, L., 1994. The Dole effect and its variations during the last 130,000 years as measured in the Vostok ice core. Global Biogeochemical Cycles 8 (3), 363–376.

Bender, M.L., Orchardo, J., Dickson, M.L., Barber, R., Lindley, S., 1999. In vitro O-2 fluxes compared with C-14 production and other rate terms during the JGOFS Equatorial Pacific experiment. Deep-Sea Research I 46 (4), 637–654.

Bender, M.L., Dickson, M.L., Orchardo, J., 2000. Net and gross production in the Ross Sea as determined by incubation experiments and dissolved O-2 studies. Deep-Sea Research II 47 (15–16), 3141–3158.

Benson, B.B., Krause, D., 1984. The concentration and isotopic fractionation of oxygen dissolved in fresh-water and seawater in equilibrium with the atmosphere. Limnology and Oceanography 29 (3), 620–632.

Blunier, T., Barnett, B., Bender, M.L., Hendricks, M.B., 2002. Biological oxygen productivity during the last 60,000 years from triple oxygen isotope measurements. Global Biogeochemical Cycles 16 (3), doi: 10.1028/2001GB001460.

Bronk, D.A., Ward, B.B., 2000. Magnitude of dissolved organic nitrogen release relative to gross nitrogen uptake in marine systems. Limnology and Oceanography 45 (8), 1879–1883.

Buesseler, K.O., Ball, L., Andrews, J., Cochran, J.K., Hirschberg, D.J., Bacon, M.P., Fleer, A., Brzezinski, M., 2001. Upper ocean export of particulate organic carbon and biogenic silica in the Southern Ocean along 170°W. Deep-Sea Research II 48 (19–20), 4275–4297.

Craig, H., Hayward, T., 1987. Oxygen supersaturation in the ocean: biological versus physical contributions. Science 235 (4785), 199–202.

Dickson, M.L., Orchardo, J., 2001. Oxygen production and respiration in the Antarctic Polar Front region during the

austral spring and summer. Deep-Sea Research II 48 (19–20), 4101–4126.

Elskens, M., Baeyens, W., Cattaldo, T., Dehairs, F., Griffiths, B., 2002. N uptake conditions during summer in the Subantarctic and Polar Frontal Zones of the Australian sector of the Southern Ocean. Journal of Geophysical Research—Oceans 107(C11), Art. No. 3182.

Emerson, S., 1987. Seasonal oxygen cycles and biological new production in surface waters of the Sub-Arctic Pacific-Ocean. Journal of Geophysical Research—Oceans 92 (C6), 6535–6544.

Emerson, S., Quay, P.D., Stump, C., Wilbur, D., Schudlich, R., 1995. Chemical tracers of productivity and respiration in the Subtropical Pacific-Ocean. Journal of Geophysical Research—Oceans 100 (C8), 15873–15887.

Eppley, R.W., Peterson, B.J., 1979. Particulate organic-matter flux and planktonic new production in the deep ocean. Nature 282 (5740), 677–680.

Froneman, P.W., Laubscher, R.K., McQuaid, C.D., 2001. Size-fractionated primary production in the south Atlantic and Atlantic sectors of the Southern Ocean. Journal of Plankton Research 23 (6), 611–622.

Guy, R.D., Fogel, M.L., Berry, J.A., 1993. Photosynthetic fractionation of the stable isotopes of oxygen and carbon. Plant Physiology 101 (1), 37–47.

Kiddon, J., Bender, M.L., Orchardo, J., Caron, D.A., Goldman, J.C., Dennett, M., 1993. Isotopic fractionation of oxygen by respiring marine organisms. Global Biogeochemical Cycles 7 (3), 679–694.

Kirkwood, D.S., 1992. Stability of solutions of nutrient salts during storage. Marine Chemistry 38, 151–164.

Kroopnick, P., Craig, H., 1972. Atmospheric oxygen—isotopic composition and solubility fractionation. Science 175 (4017), 54–55.

Kroopnick, P., Craig, H., 1976. Oxygen isotope fractionation in dissolved-oxygen in the deep-sea. Earth and Planetary Science Letters 32 (2), 375–388.

Lämmerzahl, P., Röckmann, T., Brenninkmeijer, C.A.M., Krankowshy, D., Mauersberger, K., 2002. Oxygen isotope composition of stratospheric carbon dioxide. Geophysical Research Letters 29 (12), Art. No. 1582.

Lane, G.A., Dole, M., 1956. Fractionation of oxygen isotopes during respiration. Science 123 (3197), 574–576.

Laws, E.A., 1991. Photosynthetic quotients, new production and net community production in the open ocean. Deep-Sea Research I 38 (1), 143–167.

Laws, E.A., Falkowski, P.G., Smith, W.O., Ducklow, H., McCarthy, J.J., 2000a. Temperature effects on export production in the open ocean. Global Biogeochemical Cycles 14 (4), 1231–1246.

Laws, E.A., Landry, M.R., Barber, R.T., Campbell, L., Dickson, M.L., Marra, J., 2000b. Carbon cycling in primary production bottle incubations: inferences from grazing experiments and photosynthetic studies using C-14 and O-18 in the Arabian Sea. Deep-Sea Research II 47 (7–8), 1339–1352.

Lourey, M.J., Trull, T.W., 2002. Seasonal nutrient depletion and carbon export in the Subantarctic and Polar Frontal Zones of the Southern Ocean south of Australia. Journal of Geophysical Research—Oceans 106 (C12), 31463–31487.

Luz, B., Barkan, E., 2000. Assessment of oceanic productivity with the triple-isotope composition of dissolved oxygen. Science 288 (5473), 2028–2031.

Luz, B., Barkan, E., Bender, M.L., Thiemens, M.H., Boering, K.A., 1999. Triple-isotope composition of atmospheric oxygen as a tracer of biosphere productivity. Nature 400 (6744), 547–550.

Mengesha, S., Dehairs, F., Fiala, M., Elskens, M., Goeyens, L., 1998. Seasonal variation of phytoplankton community structure and nitrogen uptake regime in the Indian Sector of the Southern Ocean. Polar Biology 20 (4), 259–272.

Miller, M.F., 2002. Isotopic fractionation and the quantification of O-17 anomalies in the oxygen three-isotope system: an appraisal and geochemical significance. Geochimica et Cosmochimica Acta 66 (11), 1881–1889.

Moore, J.K., Abbott, M.R., 2000. Phytoplankton chlorophyll distributions and primary production in the Southern Ocean. Journal of Geophysical Research—Oceans 105 (C12), 28709–28722.

Moore, J.K., Abbott, M.R., Richman, J.G., 1999. Location and dynamics of the Antarctic Polar Front from satellite sea surface temperature data. Journal of Geophysical Research—Oceans 104 (C2), 3059–3073.

Morrison, J.M., Gaurin, S., Codispoti, L.A., Takahashi, T., Millero, F.J., Gardner, W.D., Richardson, M.J., 2001. Seasonal evolution of hydrographic properties in the Antarctic circumpolar current at 170°W during 1997–1998. Deep-Sea Research II 48 (19–20), 3943–3972.

Nelson, D.M., Anderson, R.F., Barber, R.T., Brzezinski, M.A., Buesseler, K.O., Chase, Z., Collier, R.W., Dickson, M.L., Francois, R., Hiscock, M.R., Honjo, S., Marra, J., Martin, W.R., Sambrotto, R.N., Sayles, F.L., Sigmon, D.E., 2002. Vertical budgets for organic carbon and biogenic silica in the Pacific sector of the Southern Ocean, 1996–1998. Deep-Sea Research II 49 (9–10), 1645–1674.

Orsi, A.H., Whitworth, T., Nowlin, W.D., 1995. On the meridional extent and fronts of the Antarctic Circumpolar Current. Deep-Sea Research I 42 (5), 641–673.

Patterson, S.L., Whitworth, T., 1990. Physical oceanography. In: Glasby, G.P. (Ed.), Antarctic Sector of the Pacific, vol. 51. Amsterdam, Elsevier, pp., 55–93.

Pollard, R.T., Lucas, M.I., Read, J.F., 2002. Physical controls on biogeochemical zonation in the Southern Ocean. Deep-Sea Research II 49 (16), 3289–3305.

Quay, P.D., Emerson, S., Wilbur, D.O., Stump, C., Knox, M., 1993. The delta-O-18 of dissolved O_2 in the surface waters of the Sub-Arctic Pacific—a tracer of biological productivity. Journal of Geophysical Research—Oceans 98 (C5), 8447–8458.

Rintoul, S.R., Donguy, J.R., Roemmich, D.H., 1997. Seasonal evolution of upper ocean thermal structure between Tasmania and Antarctica. Deep-Sea Research I 44 (7), 1185–1202.

Sambrotto, R.N., Mace, B.J., 2000. Coupling of biological and physical regimes across the Antarctic Polar Front as reflected by nitrogen production and recycling. Deep-Sea Research II 47 (15–16), 3339–3367.

Smith, W.O., Anderson, R.F., Moore, J.K., Codispoti, L.A., Morrison, J.M., 2000. The US Southern Ocean Joint Global Ocean Flux Study: an introduction to AESOPS. Deep-Sea Research II 47 (15–16), 3073–3093.

Spitzer, W.S., Jenkins, W.J., 1989. Rates of vertical mixing, gas-exchange and new production—estimates from seasonal gas cycles in the upper ocean near Bermuda. Journal of Marine Research 47 (1), 169–196.

Thiemens, M.H., Jackson, T., Mauersberger, K., Schueler, B., Morton, J., 1991. Oxygen isotope fractionation in stratospheric CO_2. Geophysical Research Letters 18 (4), 669–672.

Thiemens, M.H., Jackson, T., Zipf, E.C., Erdman, P.W., Vanegmond, C., 1995. Carbon-dioxide and oxygen-isotope anomalies in the mesosphere and stratosphere. Science 270 (5238), 969–972.

Wanninkhof, R., 1992. Relationship between wind-speed and gas-exchange over the ocean. Journal of Geophysical Research—Oceans 97 (C5), 7373–7382.

Weiss, R.F., 1970. Solubility of nitrogen, oxygen and argon in water and seawater. Deep-Sea Research 17 (4), 721–735.

Young, E.D., Galy, A., Nagahara, H., 2002. Kinetic and equilibrium mass-dependent isotope fractionation laws in nature and their geochemical and cosmochemical significance. Geochimica et Cosmochimica Acta 66 (6), 1095–1104.

Yung, Y.L., Lee, A.Y.T., Irion, F.W., DeMore, W.B., Wen, J., 1997. Carbon dioxide in the atmosphere: isotopic exchange with ozone and its use as a tracer in the middle atmosphere. Journal of Geophysical Research—Atmospheres 102 (D9), 10857–10866.